JOURNAL OF GEOPHYSICAL RESEARCH, VOL. 112, A05221, doi:10.1029/2006JA012058, 2007

Click Here for Full Article

Multispacecraft observations of chorus dispersion and source location

Aaron Breneman,[1] Craig A. Kletzing,[1] Jaroslav Chum,[2] Ondrej Santolik,[3,4] Donald Gurnett,[1] and Jolene Pickett[1]

Received 8 September 2006; revised 30 January 2007; accepted 12 February 2007; published 26 May 2007.

[1] We report Cluster Wideband Data (WBD) receiver observations of correlated chorus elements with different frequency/time characteristics as seen on multiple spatially separated Cluster spacecraft. Because chorus packets disperse as they propagate, careful comparison of the signals from multiple spacecraft can provide new information about the origin of these waves. A cross-correlation analysis is used to quantify the dispersive time delay between each frequency of a chorus element as it arrives at Cluster spacecraft pairs. This data cross-correlation is then compared with a ray-tracing technique in order to identify source locations that are consistent with the observed delays. We also consider a time-variable source that emits frequencies that increase as a function of time. This frequency drift rate is adjusted to force the frequency/time variation of the simulated chorus element on a single spacecraft to match that observed. This process yields possible source locations for each spacecraft, whose location and extent are a function of the amount of source frequency emission drift. By requiring the individual spacecraft source regions to intersect with the multispacecraft source regions, a common static source region at L $\sim$ 3.9 (McIlwain parameter) and MLAT $\sim -5.9°$ (magnetic latitude) is identified for a single event (event 1) and upper and lower bounds are placed on the amount of source emission frequency drift within the source. No common source region is found for a second event (event 2).

Citation: Breneman, A., C. A. Kletzing, J. Chum, O. Santolik, D. Gurnett, and J. Pickett (2007), Multispacecraft observations of chorus dispersion and source location, *J. Geophys. Res.*, *112*, A05221, doi:10.1029/2006JA012058.

1. Introduction

[2] Chorus is a burst-like wave emission observed in the near-Earth magnetosphere outside the plasmapause. Chorus emissions are most often observed on the Earth's dawnside between 2300 and 1300 MLT [*Tsurutani and Smith*, 1974]. Chorus emissions propagate in the whistler mode and consist of two narrow frequency range bands centered at around one-half the electron gyrofrequency at the geomagnetic equator ($\omega_{ce,eq}$) of the magnetic field line on which the waves are observed [*Tsurutani and Smith*, 1974]. The upper band, if present, exists in the frequency range of $\omega/\omega_{ce,eq} \sim 0.5-0.75$ and contains discrete chorus elements rising at a few kHz/s. The lower band exists in the frequency range of $\omega/\omega_{ce,eq} \sim 0.2-0.45$ and contains both elements rising at a few kHz/s and diffuse elements.

[3] The size of the chorus source region has been continually refined over the years. *Helliwell* [1967] predicted that an equatorial source at around 4 RE would have a parallel dimension of around 1000–3000 km along the background magnetic field. The equatorial position of chorus source was later confirmed with Poynting flux measurements by *LeDocq et al.* [1998]. Recent Poynting flux and polarization measurements on board the Cluster spacecraft not only confirmed that the chorus source is located close to the equatorial plane [*Parrot et al.*, 2003; *Santolik and Gurnett*, 2003; *Santolik et al.*, 2005a] but also showed that the dimension of the chorus source region, measured along the magnetic field lines is 3000–5000 km [*Santolik et al.*, 2004]. These experimental results have been compared with the nonlinear "backward wave oscillator" theory of *Trakhtengerts et al.* [2004] yielding an excellent agreement.

[4] Early low-altitude satellite observations showed that chorus can be observed from about L = 3 to L = 8 with peak activity at L = 5 [*Gurnett and O'Brien*, 1964]. Recent data from the Double-Star spacecraft indicate that chorus events show an increased intensity at L $\geq$ 6 up to L $\leq$ 11–12 [*Santolik et al.*, 2005b]. Within this broad generation region, smaller actively emitting regions exist where wave power is being produced. The size of these regions perpendicular to the magnetic field line was

[1]Department of Physics and Astronomy, University of Iowa, Iowa City, Iowa, USA.
[2]Institute of Atmospheric Physics, Academy of Sciences of the Czech Republic, Prague, Czech Republic.
[3]Department of Mathematics and Physics, Charles University, Prague, Czech Republic.
[4]Also at Institute of Atmospheric Physics, Academy of Sciences of the Czech Republic, Prague, Czech Republic.

Copyright 2007 by the American Geophysical Union.
0148-0227/07/2006JA012058$09.00

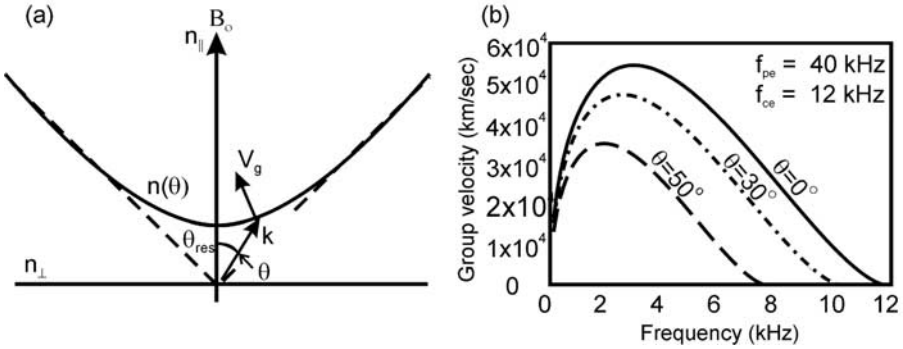

Figure 1. (a) Polar plot of the index of refraction curve $n(\theta)$ given in (1). The arrow from the origin to the curve gives the direction of the wave normal angle **k** relative to the background magnetic field B_o. The normal to the curve indicates the direction of the group velocity $\mathbf{v}_g$. The index of refraction goes to infinity at the resonance cone angles $\theta_{\rm res}$ shown as the dashed lines. (b) Plot of the group velocity (km/s) of chorus emissions as a function of frequency (kHz) for a cyclotron frequency f_{ce} = 12 kHz and a plasma frequency f_{pe} = 40 kHz for three different wave normal angles off of the background magnetic field.

estimated with a cross-correlation analysis from multiple Cluster spacecraft by *Santolik and Gurnett* [2003] and *Santolik et al.* [2004] to be of the order of the wavelength of a chorus wave packet (~100 km). In addition to being temporally dynamic in frequency and power, it is also possible that these actively emitting source regions are dynamic in position parallel to the background magnetic field, potentially moving at speeds comparable to the parallel velocity of resonant hot electrons [*Inan et al.*, 2004].

[5] It is generally agreed that chorus is generated from a nonlinear process involving whistler mode waves interacting with electrons in the energy range of 10–100 keV via a cyclotron resonance mechanism [*Kennel and Petschek*, 1966]. The exact nonlinear process by which chorus emissions are produced remains a topic of active research. *Chum et al.* [2007], in a companion paper, have shown that a quasi-stationary or static source that varies in time both the frequency of emission and the wave normal angle during the generation of a single chorus wave packet can reproduce chorus observations. We present here the identification of a static source region of chorus emission from a ray-tracing simulation for a chorus event observed on three of the four Cluster spacecraft.

2. Approach to Problem

[6] *Santolik and Parrot* [1996] have shown that chorus emissions in the magnetosphere propagate according to cold plasma theory unless the wave normal angle is extremely close to the resonance cone angle (within a half degree or less). From cold plasma theory chorus is dispersive in nature according to the following dispersion relation:

$$n^2 = 1 + \frac{\omega_{pe}^2}{\omega(\omega_{ce}\cos\theta - \omega)}, \qquad (1)$$

where n is the index of refraction, ω is the wave frequency, θ is the angle of the wave vector **k** relative to the background magnetic field B_o, ω_{pe} is the electron plasma frequency and ω_{ce} is the electron cyclotron frequency. This relation is plotted in polar coordinates in Figure 1a and for the case of $\omega_{ce}/2 > \omega > \omega_{ce}$. Note that the index of refraction goes to infinity at the resonance cone angle shown by the dashed line and defined by $\cos\theta_{res} = \omega/\omega_{ce}$. The direction of the group velocity is perpendicular to the index of refraction curve in Figure 2a. For a cold plasma the resonance cone angle can never exceed 90° relative to B_o if $\omega_{LHR} \leq \omega \leq \omega_{ce}$, where ω_{LHR} is the lower hybrid resonance frequency.

[7] Because the refractive index is frequency-dependent, different frequencies see a different refractive index for the same wave normal angle, causing chorus wave packets to spread across magnetic field lines in the same way that a prism separates frequencies of visible light. In addition, chorus shows time dispersion because of the frequency and angle dependence of the group velocity. The different curves in Figure 2b represent the group velocity of chorus emitted at three different wave normal angles. As the angle relative to the magnetic field approaches the resonance cone the group velocity slows and eventually reaches zero at the resonance cone angle. Two different frequencies emitted at two different wave normal angles from the same spatial location can arrive at a common destination at different times because of the different ray path lengths that arise due to these refractive properties. A spacecraft at a large distance from any chorus source that instantaneously generates a range of frequencies will typically measure a rising tone in the upper band because higher frequencies propagate more slowly than lower frequencies.

[8] Current models of chorus generation suggest that the range of frequencies within a given chorus element are not emitted simultaneously but rather that the emission of a given frequency is time-dependent such that higher frequencies are emitted with a delay relative to lower frequencies [*Trakhtengerts*, 1999]. We will refer to this hereafter as the source emission frequency drift. Chorus elements are often observed as rising elements (Figure 3) because the source emission frequency drift combines with the effects of dispersion.

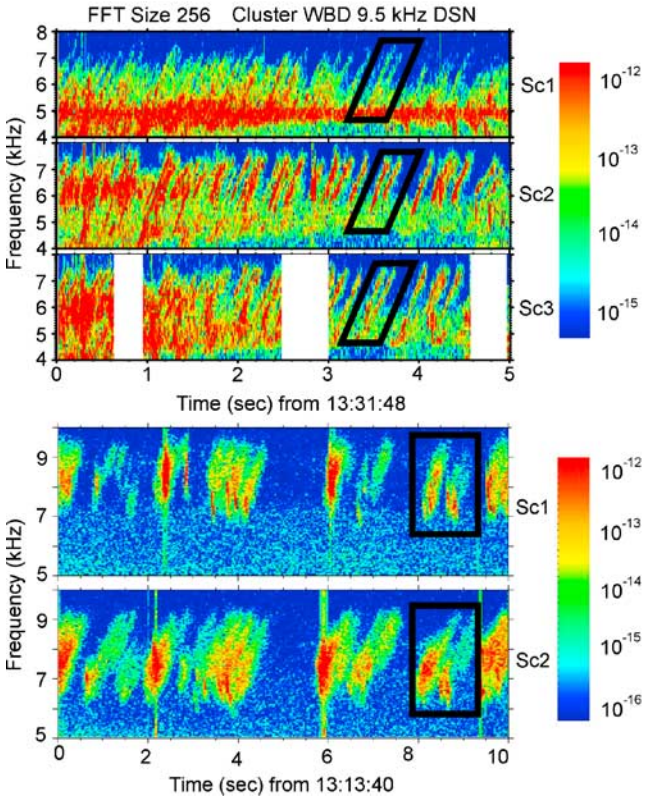

Figure 2. (a) The boxed double event is event 1 as observed on the Wideband Data instrument on Cluster spacecraft 1, 2, and 3 on 27 November 2000 at ~1331:51 UT in the form of a frequency (kHz) vs time (s) spectrogram. The spacecraft are at L ~ 3.8, lat ~ 12° and MLT ~ 6.6. The color bar shows the electric field wave power in $mV^2/m^2/Hz$. (b) Event 2 as seen on Cluster spacecraft 1 and 2 at a location of L ~ 3.8 RE, lat ~ −0.5°, and MLT ~6.6.

[9] The identification of the source region of the chorus emissions requires the separation of the source emission frequency drift from the frequency dispersion by propagation. This is accomplished by simulating both the single spacecraft Cluster Wideband Data (WBD) observations and the time of arrival difference for each frequency between spacecraft pairs (cross-correlation) with a ray-tracing technique.

3. Ray-Tracing Technique

[10] In addition to frequency dispersion, plasma waves can be refracted as they pass through an inhomogeneous medium. In the Earth's magnetosphere the index of refraction under the cold plasma approximation for a given frequency and wave normal angle is a function of the magnetic field strength and the density, both of which change as a function of magnetic latitude, altitude, magnetic local time, solar wind activity, and other variables. Therefore the amount of refraction that a ray undergoes at any instant continuously changes as a ray traverses the magnetosphere.

[11] To understand how chorus propagates, we utilize a three-dimensional ray-tracing procedure described by *Santolik et al.* [2006]. This procedure is a recently updated and improved version of the original developed by *Cairo and Lefeuvre* [1986]. Under the approximation of geometrical optics, we obtain, for a given dispersion relation, a set of differential equations describing the ray trajectories [*Stix*, 1992]. These equations are numerically integrated using a fourth-order Runge-Kutta method with an adaptive integration step. As a result, we obtain the position of the ray and the corresponding wave vector as a function of time. During the integration we verify the wave-mode and convergence criteria. Additionally, in every integration step we verify that the Wentzel-Kramers-Brillouin (WKB) approximation of geometric optics is valid. This ensures that the scale of the variations of the magnetospheric density and magnetic field is greater than the wavelength of the simulated ray. The ray is not followed beyond the limit where this fundamental approximation becomes invalid.

[12] The density is represented by a diffusive equilibrium model which is calibrated at the equatorial satellite location by plasma parameters from the WHISPER instrument on board the Cluster spacecraft [*Decreau*, 2001]. The magnetic field is given by a simple dipole model. For the L-values in question (L ~ 4) the Earth's field is close to dipolar on the

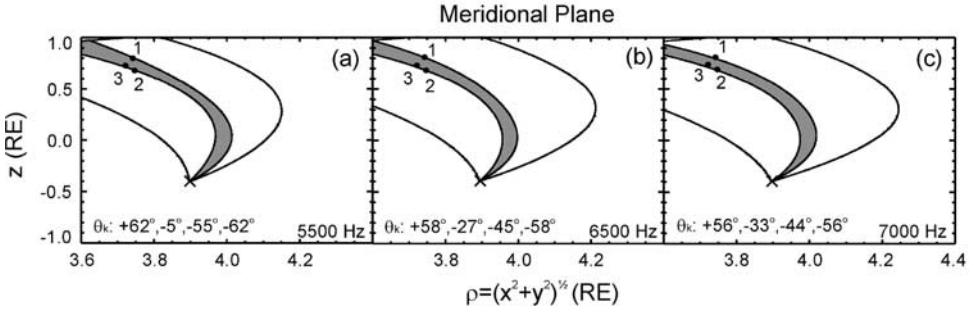

Figure 3. (a) A few 5500 Hz forward traced rays from a hypothetical source region identified as the *X* emitted toward the three spacecraft. The cartesian horizontal axis represents distance away from the Earth (RE) in the magnetic meridional plane and the cartesian vertical axis is the distance along the axis of the Earth's magnetic dipole in RE. The two extreme rays at $\theta_{\mathbf{k}} = 62°$ (leftmost) and $\theta_{\mathbf{k}} = -62°$ (rightmost) are rays near the resonance cone and the two intermediate rays at $\theta_{\mathbf{k}} = -5°$ (middle left) and $\theta_{\mathbf{k}} = -55°$ (middle right) represent the wave normal span at the source needed to illuminate all three spacecraft. (b), (c) The same as in Figure 4a but with the 6500 Hz rays and 7000 Hz rays, respectively.

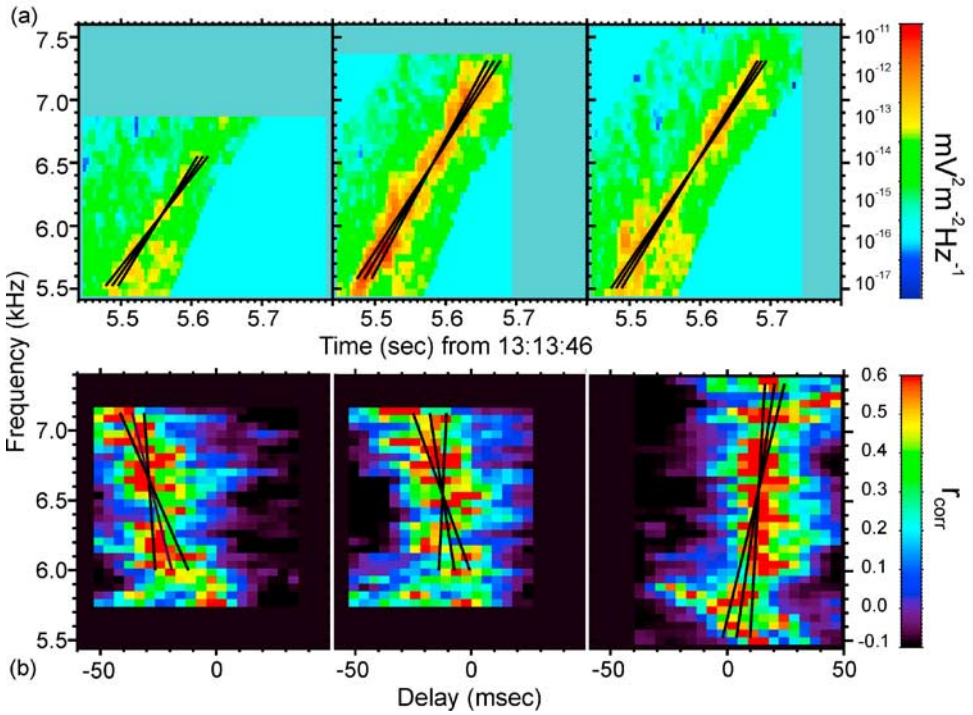

Figure 4. (a) The top row shows the frequency/time spectrogram for the first element of the double element from each box in Figure 3 of event 1 from the Wideband Data instrument on Cluster spacecraft 1, 2, and 3. The color bar shows the electric field wave power in $mV^2/m^2/Hz$. (b) The bottom row shows the cross-correlations for the double element in each box in Figure 3 for all three spacecraft pairs (sc1-sc2, sc1-sc3, and sc2-sc3, respectively) with the correlation coefficient r_{corr} shown in color. The time delays calculated from the fitted slopes are listed in Tables 2a and 2b.

dawnside except perhaps in times of extreme magnetic activity [*Ober et al.*, 2002], making this a valid approximation. The density and magnetic field models are sufficient to show the efficacy of the ray-tracing technique as a means of identifying the chorus source regions.

[13] The ray-tracing equations are reversible in time, making it possible to consider the Cluster spacecraft as the source of chorus radiation and to launch rays toward the source region. This reverse ray-tracing technique turns out to be a more convenient way to locate chorus sources as compared with forward ray-tracing.

[14] As an initial inquiry into the location of the chorus emitting regions, it is instructive to assume that the chorus source emits all appropriate frequencies simultaneously. Later on, a source emission frequency drift will be considered by delaying the emission of the higher frequency.

[15] Using reverse ray-tracing, rays are emitted in the meridional plane at the location of a single spacecraft toward the equator with the full range of allowed wave normal angles that comprise a cone that spans, in angle, from one side of the resonance cone to the other with its apex on the magnetic field line. The closest the wave vector of the simulated rays is allowed to get to the resonance cone in all cases is 5°, justifying the use of a cold plasma simulation. In the equatorial plane all rays are emitted with an angle of $\phi = 0°$. The limiting rays that reach the three spacecraft for each simulated frequency along with rays at a wave normal angle $\theta_{\mathbf{k}}$ five degrees less than the resonance cone angle are shown in Figure 4. Table 1 lists the wave normal angle and group velocity angle at both the initial position of the source and the final position of spacecraft 1 and spacecraft 2 from the ray-tracing program. Any point in space through which the rays propagate then contains information on the time of propagation from the spacecraft source to that point in space. As discussed above, this propagation time is frequency dependent.

[16] The ray-tracing timing information can be used in two ways to compare with data. First, the single spacecraft observations are simulated using the reverse ray-tracing technique. Two different frequencies are emitted from the location of a single spacecraft toward the possible source region. In the initial simulation both frequencies are emitted simultaneously. For subsequent simulations, an arbitrary source emission frequency drift is introduced by delaying the emission of the higher frequency relative to a given lower frequency. Since the two frequencies have different propagation velocities (Figure 2), there exists a propagation time difference at every location in the magnetosphere through which both rays propagate. The region of possible chorus sources for a single spacecraft is identified as the area where the simulated time difference between the two frequencies matches the observed single spacecraft slope within a 1σ variation of the best fit slope. The location and size of the simulated region of possible chorus sources for a single spacecraft is sensitive to both the dispersion delay from ray propagation and the source emission frequency drift.

[17] Second, by subtracting these propagation times for all the rays simulated at one spacecraft from those simulated

Table 1. Values of the Wave Normal Angle and the Group Velocity Angle, deg, Relative to the Ambient Magnetic Field for the Forward Ray-Tracing Simulation at Both the Position of Each Respective Spacecraft and at the Position of the Source Located at x = 3.897 RE, $lat = -5.93°$[a]

	θ_{k-sc}	θ_{vg-sc}	$\theta_{k-source}$	$\theta_{vg-source}$
sc1 5500 Hz	8.3	2.0	−55.0	−9.6
sc1 6500 Hz	37.3	−0.1	−45.0	−8.8
sc1 7000 Hz	42.3	−4.9	−44.0	−11.0
sc2 5500 Hz	57.0	−6.8	−5.0	1.0
sc2 6500 Hz	48.1	−6.0	−27.0	−0.1
sc2 7000 Hz	45.8	−7.5	−33.0	−4.4

[a]The rays that arrive at spacecraft 1 and spacecraft 2 represent the limiting rays that illuminate all three spacecraft. The plasma frequency is ω_{pe} = 49.8 kHz at the source and ω_{pe} ~51 kHz at the spacecraft.

at another spacecraft at each point in space the cross-correlation delay time for each frequency for a spacecraft pair can be simulated as a function of position. Since these cross-correlation time delays represent relative differences in ray propagation from one spacecraft to another they are independent of any source emission frequency drift. The region of possible chorus sources for each cross-correlation plot is identified as the area where the simulated cross-correlation matches the observed cross-correlation within a 1σ variation of the observed cross-correlation best fit slope. The location and size of each of these regions depends only on the dispersive frequency separation a chorus wave packet undergoes as it travels from one spacecraft to another.

[18] After all the single spacecraft and cross-correlation simulations are complete we are left with $n(n + 1)/2$ possible regions of chorus sources with which to compare with data, where n represents the number of spacecraft considered. By requiring both the single spacecraft simulations and the cross-correlation simulations to overlap, we are able to identify both the source region and the source emission frequency drift which are consistent with all aspects of the data. This source region in the meridional plane is assumed to emit waves over all azimuthal angles.

4. Analysis of Event 1

[19] The boxed chorus element in Figure 3a shows event 1 observed on the Wideband Data (WBD) instrument on Cluster spacecraft 1, 2, and 3 on 27 November 2000 at ~1331:51 UT. The spacecraft are north of the source region near L ~ 3.8, a magnetic latitude of lat ~ 12°, and at MLT ~6.6. For an initial analysis of chorus activity at this time, see *Gurnett et al.* [2001]. The separations between the spacecraft parallel to the ambient field line are sc1–sc2 ~ 800 km, sc1–sc3 ~ 500 km, and sc2–sc3 ~300 km and the separations between the spacecraft perpendicular to the ambient field line are all less than 200 km. A close inspection of Figure 3a reveals that the slope of event 1 differs between the three spacecraft. This difference is to be expected because the amount of dispersion depends on the distance the wave packet has traveled and the three spacecraft have different locations. Figure 5a shows a zoomed in view of the first of two elements in event 1 isolated from the rest of the spectrogram making the difference in slope among the three spacecraft immediately apparent.

[20] The bottom three boxes in Figure 5 are the cross-correlations for the three possible spacecraft pairs of the double element of event 1. The correlation coefficient r_{corr} is a dimensionless number ranging from −1, representing perfect anticorrelation, to 1, representing perfect correlation between two signals. In practice a single frequency channel from one spacecraft is delayed by various amounts of time relative to the same frequency channel from another spacecraft and the correlation value r_{corr} is computed for each delay time. The estimated signal delay for each channel is identified as the delay giving the highest statistically significant correlation.

[21] The slopes of the three cross-correlation pairs and of the chorus element as seen on the three single spacecraft, shown plotted in Figure 5, have been calculated using a linear least squares minimization technique. From this slope the dispersive delay between the 5500 Hz rays and the 6500 Hz rays is quantified in Tables 2a and 2b for the best fit lines and the 1σ variation from that line for each of the six plots in Figure 5. If dispersion is to account for the slope in the cross-correlation plots, these cross-correlation delay times must have a common generation region at a plausible location, that is, within a few degrees of the magnetic equator.

[22] The result of the simulation for the three spacecraft pairs for event 1 in Figure 5 is shown in Figure 1a. Rays were launched from the location of each of the three spacecraft (the symbols 1, 2, and 3) toward the source region. The three lighter colors represent the area where the ray timing delay between the 5500 Hz and the 6500 Hz rays in the cross-correlation plots at each point in space fall between the calculated variation of the slope (Δt_{min} and Δt_{max}) listed in Table 2b for the three cross-correlation pairs. The outlined white region represents the area common to the three simulations. This is identified as the region of possible chorus sources as determined by using only cross-correlation. From this plot it is seen that part of this region does lie within a few degrees of the equator. This suggests that dispersion is the primary cause of the slopes in the cross-correlation plots.

[23] However, the source region must also be consistent with the observed single spacecraft dispersion. The lower right-hand corner of Figure 1a shows the overlayed plots from the individual spacecraft within the calculated variation of the single spacecraft timing delays given in Table 2a for no source emission frequency drift, that is, all frequencies emitted simultaneously. Spacecraft 1 is shown in dark green and spacecraft 2 is shown in dark red, and no such region exists for spacecraft 3 for zero source emission frequency drift. If the model of instantaneous emission from a single source region were the case, then a region of overlap from all six areas in Figure 1a would be expected, but as is seen, there is no overlap between all six areas. The situation does not improve as the rays are allowed to approach the resonance cone closer than 5°.

[24] This suggests that it is necessary to delay the emission within the source of the higher frequencies relative to the lower frequencies. When this is done, the regions in space that can act as source regions with the measured amount of time variation shown in Table 2a for the three single spacecraft open up substantially. The source emission frequency drift can be adjusted to create an overlap of the

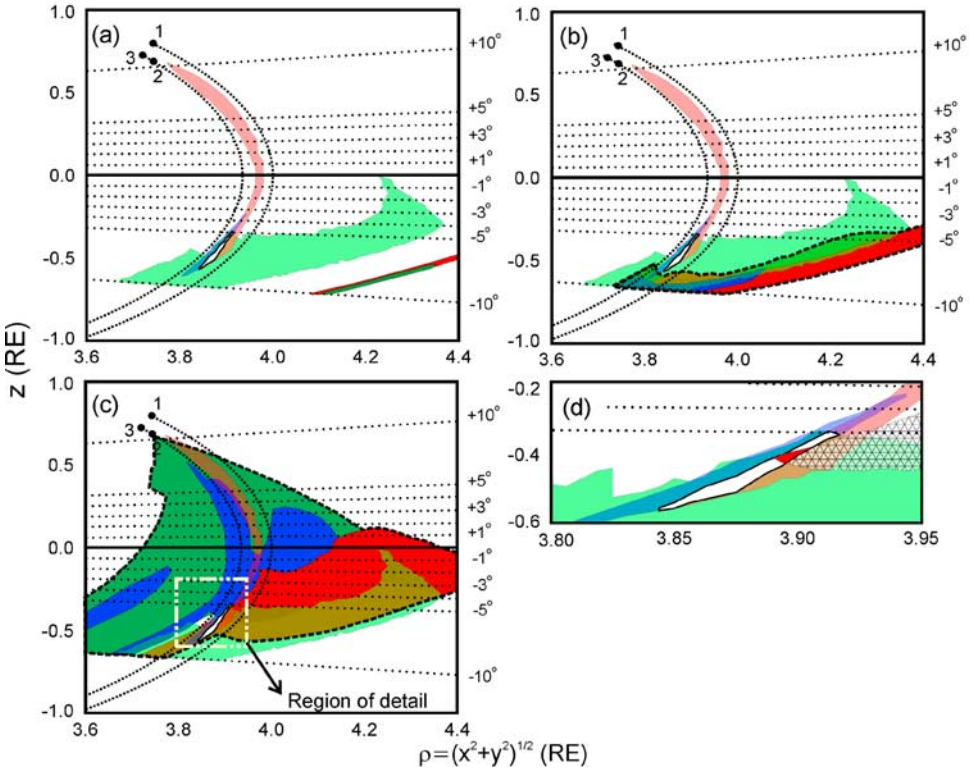

Figure 5. The cross-correlation and the single spacecraft simulation results in the meridional plane. The cartesian horizontal axis represents distance away from the Earth (RE) in the magnetic meridional plane and the cartesian vertical axis is the distance along the axis of the Earth's magnetic dipole (RE). The three spacecraft are shown by the dots next to the symbols 1, 2, and 3. The dotted lines of latitude are labeled to the right of each plot. The colored areas show the regions where the cross-correlation time delays $\Delta t_{sc1-sc2}$ (light blue), $\Delta t_{sc1-sc3}$ (light red), and $\Delta t_{sc2-sc3}$ (light green) and the single spacecraft time delays Δt_{sc1} (dark red), Δt_{sc2} (dark green), Δt_{sc3} (dark blue) are within the calculated variation of the slope of each element as listed in Tables 2a and 2b. The region of possible sources, identified by the overlap between the three cross-correlation plots, is shown by the outlined white region in the third box. (a) No source emission frequency drift, i.e., the 5500 Hz rays and the 6500 Hz rays are emitted simultaneously from the spacecraft source. Two of the three single spacecraft simulations are in the lower right corner of the figure and do not overlap with the source region when there is no source emission frequency drift. The area for spacecraft 3 does not exist in this case. (b) The same as in Figure 1a but with a source emission frequency drift of 14.2 kHz/s. (c) The same as in Figures 1a and 1b but with a source emission frequency drift of 9.6 kHz/s. (d) A zoomed-in view of the region of possible chorus sources (region of detail) identified as the area consistent with the three cross-correlation simulations in Figure 1a. The red area is identified as the source region for the 9.6 kHz/s drift.

three single spacecraft regions with the region of possible chorus sources that has been identified from the overlap of the cross-correlation plots. Figure 1b shows the result for a source emission frequency drift of 14.2 kHz/s. At this source emission frequency drift there is still no overlap between all six plots, but it is clear that the regions are moving closer to having an overlap. This overlap first occurs at a source emission frequency drift of ~12.5 kHz/s. Figure 1c shows a source emission frequency drift of 9.6 kHz/s which yields an overlap between all six regions. A zoomed in view of this source is shown in Figure 1d. Here the single spacecraft areas have been removed and replaced by the cross-hatched region showing the area of their common overlap. The solid red region is the overlap between all six plots and represents the region of possible chorus sources for a source emission frequency drift of 9.6 kHz/s. As a check, a forward ray-tracing simulation (from the source to the spacecraft) was then performed at the location of the source region (shown in red) for the 9.6 kHz/s source emission frequency drift in Figure 1d. The

Table 2a. Here Δt is the Time Difference in Arrival, ms, Between the 6500 Hz Ray and the 5500 Hz Ray As Indicated By the Slopes in Figure 5a for Each Single Spacecraft and Δt_{max} and Δt_{min} Show This Time Difference for the Two 1σ Variations of the Slope

	sc1	*sc2*	*sc3*
Δt	127	107	115
Δt_{min}	111	95	108
Δt_{max}	143	119	123
Slope best fit	f = 7.89t-37.8	f = 9.33t-45.7	f = 8.64t-41.9
1σ slope for t_{min}	f = 9.02t-44.1	f = 10.44t-51.8	f = 9.24t-45.2
1σ slope for t_{max}	f = 7.01t-32.9	f = 8.44t-40.7	f = 8.11t-38.9

Table 2b. Same As in Table 2a But for the Cross-Correlation Plots in Figure 5b

	sc1-sc2	*sc1-sc3*	*sc2-sc3*
Δt	−15.27	−9.42	8.97
Δt_{min}	−26.32	−21.74	3.43
Δt_{max}	−4.21	2.9	14.5
Slope best fit	f = −0.066t + 4.5	f = −0.106t + 4.96	f = 0.111t + 5.31
1σ slope for t_{min}	f = −0.038t + 5.43	f = −0.046t + 5.84	f = 0.069t + 5.79
1σ slope for t_{max}	f = −0.237t-0.82	f = 0.344t + 11.56	f = 0.291t + 3.30

slope at the position of the three spacecraft created by the different arrival times of the 5500 Hz ray and the 6500 Hz ray is shown as the three dotted white lines overlayed with the 1σ lines centered on a common starting time in Figure 6. As is expected, the slopes at the positions of the three spacecraft fall within the slope uncertainty.

5. Analysis of Event 2

[25] Figure 3b shows another correlated event (event 2) as observed by Cluster spacecraft 1 and 2 on 27 November 2000 at ~1313:48 UT, 6.7 MLT and at around −2° latitude. Event 2 takes place about 18 min prior to event 1. The cross-correlation delay of this event between spacecraft 1 and 2 is shown in Figure 7 and Table 3. The x-axis is the delay in ms of arrival for a single frequency between spacecraft 1 and 2. The cross-correlation is simulated by launching rays toward the source region in the same way as was done for event 1. Simulation results show that there are no areas in the magnetosphere within 15° of the equator (where the rays were artificially limited in the simulation) that are consistent with the 1σ variation of the calculated best fit slope of the cross-correlation. This suggests that another process, along with dispersion, is separating the different frequencies.

6. Discussion

[26] An overlap between all six plots first occurs in event 1 for a source emission frequency drift of ~12.5 kHz/s and is last seen at a source emission frequency drift of ~9.5 kHz/s. These values are in reasonable agreement with Cluster observations of 15 kHz/s and the theory of the frequency drift rate from the Backward Wave Oscillator model calculated to be 7 kHz/s [*Trakhtengerts et al.*, 2004]. No source within the possible chorus generation region is identified for event 2. Events 1 and 2 represent two types of chorus elements commonly seen in the magnetosphere. Chorus events similar in nature to event 1 can be explained simply as a result of dispersive effects combined with a modest source emission frequency drift. However, the cross-correlation of event 2 between Cluster spacecraft 1 and 2 indicates that something in addition to dispersion is delaying the arrival of each frequency from one spacecraft to the other. *Inan et al.* [2004] has proposed that a rapidly moving chorus source would introduce a Doppler shift between a single chorus element observed on two spacecraft with different lines of sight to the source. In a companion paper [*Chum et al.*, 2007] we propose an alternative explanation of these large time delays and frequency differences between the corresponding chorus elements observed on different spacecraft. We show that a quasi-static source that emits waves in a relatively narrow interval of wave normal angles and that varies both the wave normal angle and frequency during the generation of a single chorus element can reproduce these observations. To demonstrate this hypothesis, we performed a ray tracing analysis from a source located close to geomagnetic equator checking the arrival times and frequencies at the locations of individual spacecraft.

Table 3. Here Δt is the Time Difference in Arrival, ms, Between the 8500 Hz Ray and the 7000 Hz Ray in the sc1-sc2 Cross-Correlation for Event 2 in Figure 7 and Δt_{max} and Δt_{min} Show This Time Difference for the Two 1σ Variations of the Slope

Variable	Value
Δt	416
Δt_{min}	385
Δt_{max}	455
Slope best fit	f = 0.0036t + 7.59
1σ slope for t_{min}	f = 0.0039t + 7.56
1σ slope for t_{max}	f = 0.0033t + 7.64

7. Conclusions

[27] We have demonstrated that a reverse ray-tracing technique can be used to identify a region of possible chorus sources for one type of event on the Cluster spacecraft. This technique identifies a source located at ~−5.9° latitude and which has a range of source emission frequency drifts of 9.5–12.5 kHz/s. This region is consistent

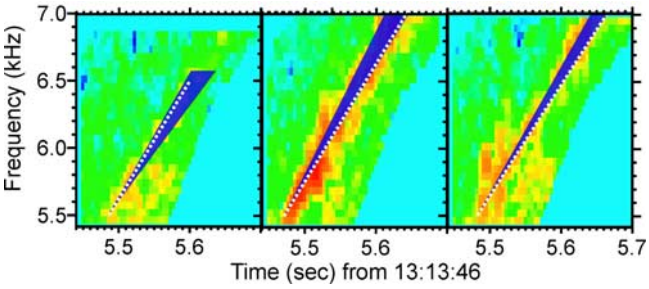

Figure 6. A plot of the 1σ lines for the three single spacecraft adjusted to a common starting time. The dotted line overlayed is the slope observed at each spacecraft from the forward traced rays launched from a point within the estimated source for a source emission frequency drift of 9.6 kHz/s (identified in Figure 1d). The coordinates of the source for this case are at x = 3.897 RE and lat ~ −5.93°. As is expected the dotted lines fall within the error of the possible slopes of each chorus element.

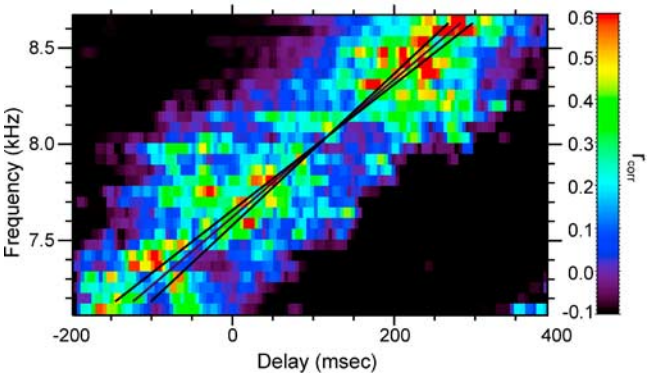

Figure 7. The cross-correlation (frequency (kHz) versus delay (ms)) from the Cluster Wideband Data instrument for each frequency as seen on spacecraft 1 and 2 for event 2 in Figure 3b. The color represents the correlation coefficient r_{corr} which ranges from unity for perfect correlation to zero for no correlation. The equations of the best fit line and the 1σ variations off of the best fit line are given in Table 3.

with experimental observations in both its location in the magnetosphere and its range of source emission frequency drift rates. The same technique however, was not successful toward identifying a source region for event 2 suggesting more complex source characteristics in some cases.

[28] **Acknowledgments.** We thank P. Canu for estimation of plasma density from Whisper data. This research was supported by the NASA Goddard Space Flight Center under grant NNG04GB98G and by the NASA Graduate Student Research Program (GSRP) under grant NNG05GN92H.

[29] Zuyin Pu thanks Pierrette Decreau and another reviewer for their assistance in evaluating this paper.

References

Cairo, L., and F. Lefeuvre (1986), Localization of sources of ELF/VLF hiss observed in the magnetosphere: Three-dimensional ray-tracing, *J. Geophys. Res.*, *91*, 4352–4364.

Chum, J., O. Santolik, A. Breneman, and C. Kletzing (2007), Chorus source properties that produce time shifts and frequency range differences observed on different Cluster spacecraft, *J. Geophys. Res.*, doi:10.1029/2006JA012061, in press.

Decreau, P. (2001), Early results from the Whisper instrument on Cluster: An overview, *Ann. Geophys.*, *19*, 1241–1258.

Gurnett, D., and B. O'Brien (1964), High-latitude geophysical studies with satellite Injun 3, *J. Geophys. Res.*, *69*, 65–89.

Gurnett, D., R. Huff, and J. Pickett (2001), First results from the Cluster Wideband Plasma Wave Investigation, *Ann. Geophys.*, *19*, 1259–1272.

Helliwell, R. (1967), A theory of discrete VLF emissions from the magnetosphere, *J. Geophys. Res.*, *72*, 4773–4790.

Inan, U., M. Platino, T. Bell, D. Gurnett, and J. Pickett (2004), Cluster measurements of rapidly moving sources of ELF/VLF chorus, *J. Geophys. Res.*, *109*, A05214, doi:10.1029/2003JA010289.

Kennel, C., and H. Petschek (1966), Limit on stably trapped particle fluxes, *J. Geophys. Res.*, *71*, 1–28.

LeDocq, M., D. Gurnett, and G. Hospodarsky (1998), Chorus source locations from VLF Poynting flux measurements with the Polar spacecraft, *Geophys. Res. Lett.*, *25*, 4063–4066.

Ober, D., M. Thomsen, and N. Maynard (2002), Observations of bow shock and magnetopause crossings from geosynchronous orbit on 31 March 2001, *J. Geophys. Res.*, *107*(A8), 1206, doi:10.1029/2001JA000284.

Parrot, M., O. Santolik, N. Cornilleau-Wehrlin, M. Maksimovic, and C. Harvey (2003), Source location of chorus emissions observed by Cluster, *Ann. Geophys.*, *21*, 473–480.

Santolik, O., and D. Gurnett (2003), Transverse dimensions of chorus in the source region, *Geophys. Res. Lett.*, *30*(2), 1031, doi:10.1029/2002GL016178.

Santolik, O., and M. Parrot (1996), The wave distribution function in a hot magnetospheric plasma: The direct problem, *J. Geophys. Res.*, *101*, 10,639–10,651.

Santolik, O., D. Gurnett, J. Pickett, M. Parrot, and N. Cornilleau-Wehrlin (2004), A microscopic and nanoscopic view of storm-time chorus on 31 March 2001, *Geophys. Res. Lett.*, *31*, L02801, doi:10.1029/2003GL018757.

Santolik, O., D. Gurnett, J. Pickett, M. Parrot, and N. Cornilleau-Wehrlin (2005a), Central position of the source region of storm-time chorus, *Planet. Space Sci.*, *53*, 299–305.

Santolik, O., E. Macusova, K. Yearby, H. S. Alleyne, and N. Cornilleau-Wehrlin(2005b), Radial variation of whistler-mode chorus: First results from the STAFF/DWP instrument onboard the Double Star TC 1 spacecraft, *Ann. Geophys.*, *23*, 2937–2942.

Santolik, O., J. Chum, M. Parrot, D. Gurnett, J. Pickett, and N. Cornilleau-Wehrlin (2006), Propagation of whistler-mode chorus to low altitudes: Spacecraft observations of structured ELF hiss, *J. Geophys. Res.*, *111*, A10208, doi:10.1029/2005JA011462.

Stix, T. (1992), *Waves in Plasma*, Springer, New York.

Trakhtengerts, V. (1999), A generation mechanism for chorus emission, *Ann. Geophys.*, *17*, 95–100.

Trakhtengerts, V., A. Demekhov, E. Titova, B. Kozelov, O. Santolik, D. Gurnett, and M. Parrot (2004), Interpretation of Cluster data on chorus emissions using the backward wave oscillator model, *Phys. Plasmas*, *11*(4), 1345–1351, doi:10.1063/1.1667495.

Tsurutani, and Smith (1974), Postmidnight chorus: A substorm phenomenon, *J. Geophys. Res.*, *79*, 118–127.

A. Breneman, D. Gurnett, C. A. Kletzing, and J. Pickett, Department of Physics and Astronomy, University of Iowa, Iowa City, IA 52242-1479, USA. (awbrenem@hotmail.com)

J. Chum, Institute of Atmospheric Physics, Academy of Sciences of the Czech Republic, Prague, Czech Republic.

O. Santolik, Department of Mathematics and Physics, Charles University, Prague, Czech Republic.